

THERMAL ANALYSIS—THEORY AND APPLICATIONS IN METALCASTING

Doru M. Stefanescu

The Ohio State University, Columbus, OH, USA
The University of Alabama, Tuscaloosa, AL, USA

Copyright © 2015 American Foundry Society

Abstract

Monitoring and adjusting the chemical composition and the nucleation potential of casting alloys melts is critical to the production of castings of consistent high quality. While other methods such as fractured test samples (e.g., the wedge test for gray iron) and spectrographic chemical analysis deliver useful information, thermal analysis (TA) (also called cooling curve analysis, CCA) can provide a more complete insight in the dynamic changes occurring upon melting and during melt treatment of casting alloys. Initially TA was used for the rapid evaluation of the carbon equivalent (CE) in cast iron, or the silicon content in Al-Si alloys. Extensive research then extended the capabilities of TA to the understanding of the solidification changes induced by compositional variations such as the Mn/S ratio, Ce and Mg additions. With the advent of ever faster computers, the first derivative of the cooling curve, which is the cooling rate, was added to the arsenal of data provided by TA, and a new technique, Computer Aided Cooling Curve Analysis (CA-CCA), was born. This

technique evolved then into Differential Thermal Analysis (DTA) without a reference sample. With this tool in hand the metallurgist ventured to predict not only the chemistry of the melt but also the nucleation potential (degree of inoculation), the shrinkage propensity, the dendrite arm spacing and the grain size, the graphite shape, the solidification microstructure, and even the room temperature microstructure. Currently, different TA techniques are used worldwide in the daily production of all grades of cast iron, as well as in monitoring the melting of aluminum and steel alloys.

From this short introduction it should be obvious that the story of DTA/CCA is a long and exciting one. This paper will try to summarize the fascinating development and extraordinary success of this technique in the casting industry.

Keywords: thermal analysis, cooling curve analysis, differential thermal analysis, cast iron, aluminum alloys

Background

Thermal Analysis (TA) is the recording and interpretation of the temperature variation in time of a cooling or heated material. In its simplest form, as applied to metalcasting, the cooling curve of a metal solidifying in a mold is recorded and analyzed (CCA). Its interpretation is based on the belief that all the events occurring during solidification leave their mark on the shape of the cooling curve. It appears that Le Chatelier was the first scientist that recorded temperature as a function of time in heating curves in 1887.¹

Differential Thermal Analysis (DTA), which consists of time, temperature and temperature difference measurements, appears to have been performed first by Roberts-Austen² in 1899, with equipment developments by Kurnakov³ and Saladin.⁴ Differential Thermal Analysis can be conducted with or without a reference body and using one or two thermocouples in the same test mold. The reference body is a material, real or virtual (computer-generated) that has no phase transformation over the temperature interval of interest.

Cooling curve analysis has evolved over the years becoming a powerful tool for casting process control. The application of CCA to cast iron appears to have started in 1931 by Esser and Lautenbusch⁵ who showed that increasing the superheating of gray iron depresses the eutectic arrest (Fig. 1). Qualitative observations were also made by Piwowarski,⁶ who noticed that higher silicon decreases the undercooling (Fig. 2), by Loper et al.,⁷ who observed the effect of the Mn/S ratio on the eutectic undercooling (Fig. 3), and by Naro and Wallace⁸ who revealed the effect of cerium and sulfur additions (Fig. 4). De Sy and Vidts⁹ pointed out that cooling curves contain information on graphite shape.

Today, TA can be used to predict alloy composition, grain refining in steel, aluminum, magnesium and other alloys, eutectic morphology (e.g., graphite morphology in cast irons or degree of modification in Al alloys) and shrinkage propensity. Computer analysis of the cooling curve can provide quantitative information on solidification, such as latent heat of solidification, evolution of fraction solid, amounts of phases, dendrite coherency and dendrite arm spacing.

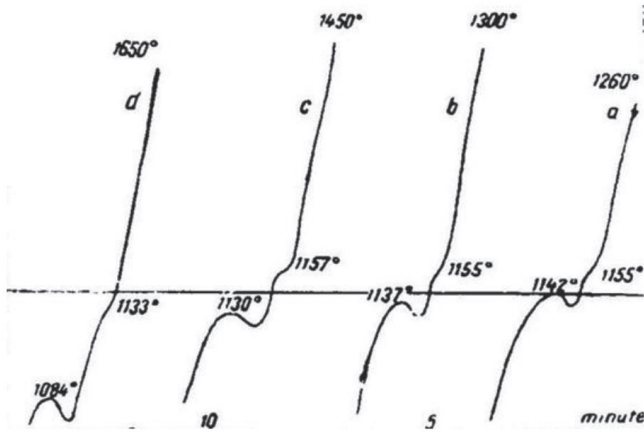


Figure 1. Effect of superheating on the eutectic temperature of gray iron (after Esser and Lautenbusch).

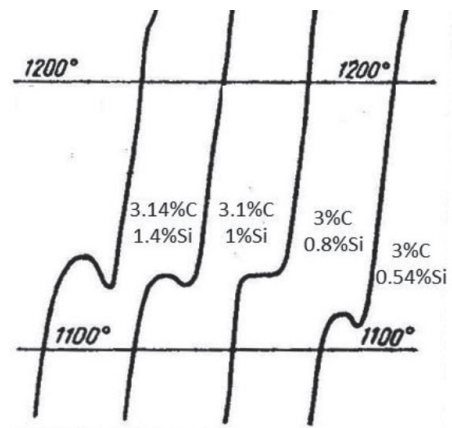


Figure 2. Effect of silicon on the eutectic temperature of gray iron.⁶

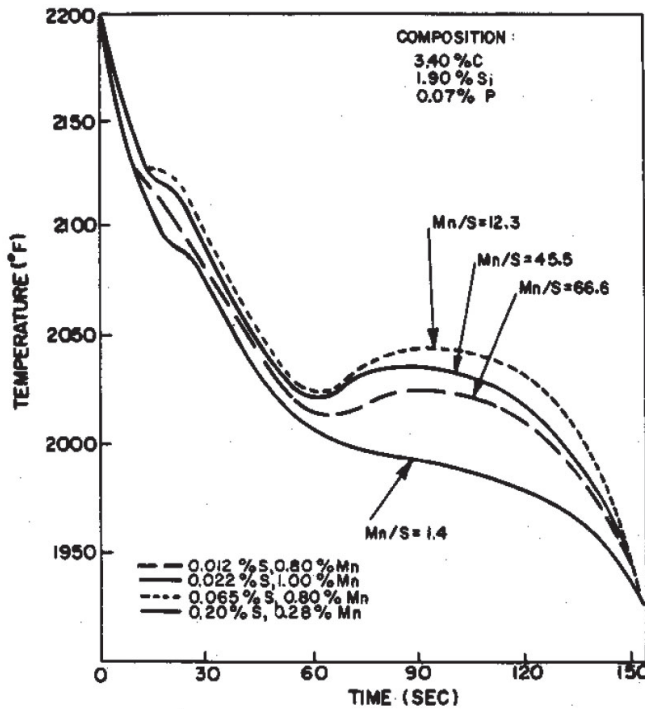


Figure 3. Effect of the Mn/S ratio on gray iron cooling curves.⁷

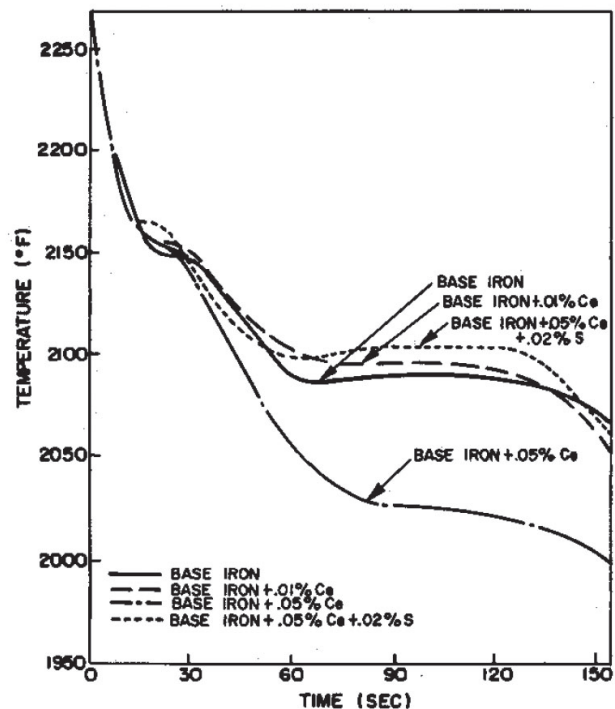


Figure 4. Effect of the Ce and S additions on gray iron cooling curves.⁸

Direct Thermal Analysis

In its simplest form TA/CCA uses one thermocouple inserted in the test mold. The design of the test cup has a significant effect on the results and their interpretation. The shape of the cooling curve is determined by the balance between the latent heat liberated during solidification and the heat lost to the surroundings (test cup and atmosphere). It is important that the design of the cup guarantees consistent sampling conditions. The cooling curve is affected by the pouring temperature, the amount of metal poured and the degree of oxidation of the metal in the cup. A faster cooling because of a smaller test sample will alter the solidification behavior of the iron, affecting the undercooling. As shown in Fig. 5, as the size of the cup decreases, undercooling increases. The effect of inoculation is more noticeable on the smaller size cups.

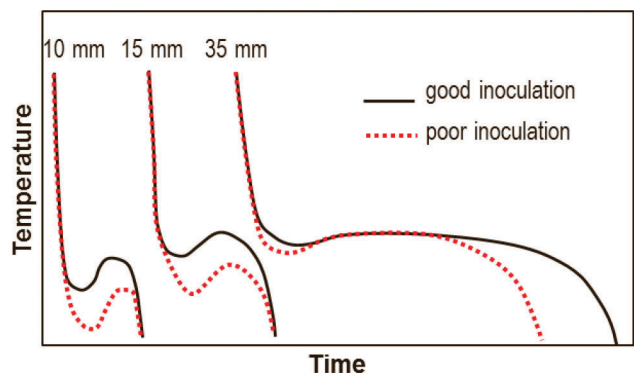


Figure 5. Schematic representation of the effect of cup size and inoculation on the shape of the cooling curve.

Instrumentation and Thermiology

Two types of cups are currently widely used in casting practice: sand cups and metal cups (see examples in Fig. 6). Sand cups are cheaper, but a metal cup allows for a more precise positioning of the thermocouple and more consistent filling. Figure 7 shows the cooling curves for lamellar graphite (LG), compacted graphite (CG) and spheroidal graphite (SG) irons with the same carbon equivalent but poured in cups of different materials. Note that for the metal cup, SG

had the highest undercooling, and using the sand cup,¹¹ CG exhibited the highest undercooling.

A combination of number of cups and number of thermocouple per cup are used, as follows:

- 1 test cup with one thermocouple (TC) (Fig. 6a)
- 2 test cups, 1 TC per cup
- 3 test cups, 1 TC per cup (Fig. 8)
- 1 test cup, 2 TCs (e.g., Fig. 6b)

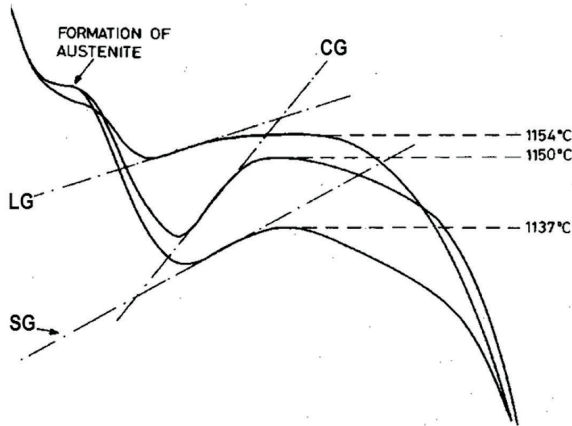


a) sand cup with disposable thermocouple

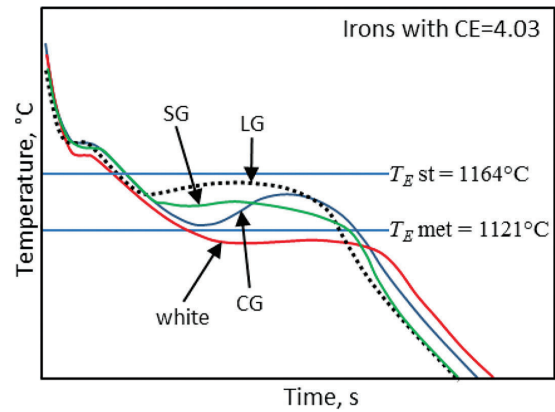


b) steel cup (SinterCast) with two thermocouples in the protective tube

Figure 6. Examples of the test cups used for cooling curve analysis.



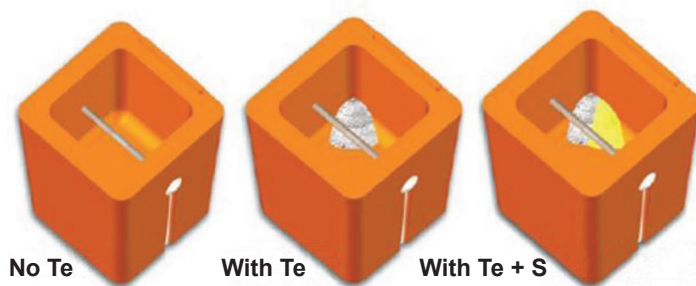
a) metal cup



b) sand cup

Figure 7. Cooling curves for three types of irons obtained with different types of cups with a single thermocouple.

Figure 8. Three cups with one thermocouple each for evaluation of Mg content in ductile iron.¹⁷



The standard terminology used in CCA is introduced in Fig. 9 as follows: T_L - equilibrium liquidus temperature, T_E - equilibrium eutectic temperature, T_{LA} - temperature of liquidus arrest, T_{Emin} - temperature of eutectic undercooling, T_{Emax} - temperature of eutectic recalescence, ΔT - recalescence, ΔT_{max} - maximum undercooling, ΔT_{min} - minimum undercooling.

Estimation of Chemical Composition

Because of the direct correlation between transformation temperatures and composition, TA has been used extensively to build phase diagrams. The first application of CCA in process control was to evaluate the carbon equivalent of cast iron and the silicon content in Al-Si alloys. It is based on the correlation between the liquidus temperature of an alloy (T_L) and its chemical composition (%C), as illustrated in Figure 10. However, because solidification is a non-equilibrium process, the real cooling curve will be quite different from the theoretical one. It will exhibit undercooling with respect to the equilibrium temperatures, as shown on the same figure. Thus, the thermodynamic equilibrium liquidus temperature will be in most cases higher than the actual non-equilibrium temperature measured by the thermocouple.

For the case of cast iron the application of this principle is based on the concept of carbon equivalent, CE , that includes the contribution of carbon and of the other important elements (Si, Mn, P, S, etc.), allowing the multicomponent iron to be treated like a binary Fe-C alloy. It can be calculated from equilibrium thermodynamics. However, because of the discrepancy between the theoretical and actual curve, Humphreys¹² has introduced the Carbon Equivalent Liquidus (CEL) that is different than the thermodynamic eutectic CE , which is calculated as $CE = \%C + 0.31\%Si + 0.33\%P - 0.027\%Mn + 0.4\%S$ (see Reference 13 for details). Based on large number of experiments with standardized test molds (sand cups) the following correlations were established:

$$T_{LA} = 1669 - 124 \cdot CEL$$

Where; $CEL = \%C + \%Si/4 + \%P/2$ Eqn. 1

A correlation between composition and the liquidus arrest temperature (in °C) was also established by Heine^{14,15} for hypoeutectic gray irons:

$$T_{LA} = 1569 - 97.3(\%C + 0.25 \cdot \%Si)$$
 Eqn. 2

Further work¹⁶ at BCIRA in England used two cups, a standard cup and a cup that had a tellurium addition, resulted in the ability to determine both C and Si from CCA. The tellurium addition had the effect of promoting metastable (white) solidification which, due to the high growth rate of the white eutectic (ledeburite) all but eliminates the eutectic undercooling. The eutectic arrest, TE_{white} , becomes flat. The equations proposed by Heraeus Electro-Nite¹⁷ are:

$$CEL = 14.45 - 0.0089 \cdot TL$$

$$\%C = -6.51 - 0.0084 \cdot TL + 0.0178 \cdot TE_{white}$$

$$\%Si = 78.411 - 4.28087 \cdot Si-adj. - 0.06831 \cdot TE_{white}$$
Eqn. 3

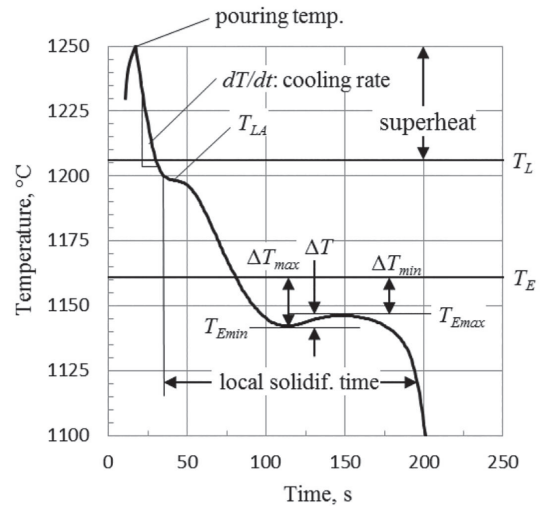


Figure 9. Typical terminology used in TA for casting process control.

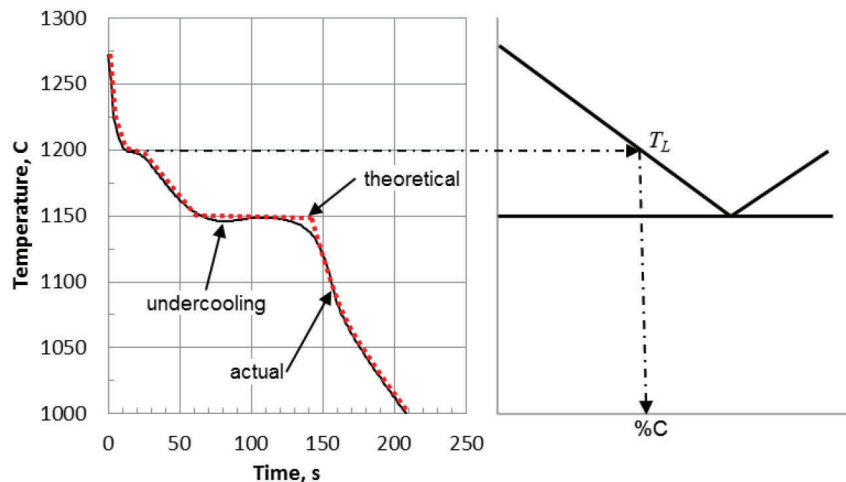


Figure 10. Theoretical (equilibrium) and experimental (non-equilibrium) cooling curves for a hypoeutectic alloy.

Where; Si_{adj} is a correction factor, mainly depending on the phosphorus content of the iron. For SG iron the same equation as for LG iron can be used to calculate CEL by substituting TL with $(TL + 5)$.

A three-cup system was also used to determine the magnesium content of Mg treated irons. The system includes a standard cup, one with tellurium, and one with tellurium and sulfur (Fig. 8).

Predicting Eutectic Type and Degree of Inoculation in Cast Iron

Another application of single thermocouple TA in cast iron is for the prediction of the general eutectic structure, *i.e.*, gray (stable) or white (metastable). If both the start and end of eutectic solidification are above the metastable temperature, T_{met} , the iron solidifies gray, *i.e.*, without carbides (Fig.

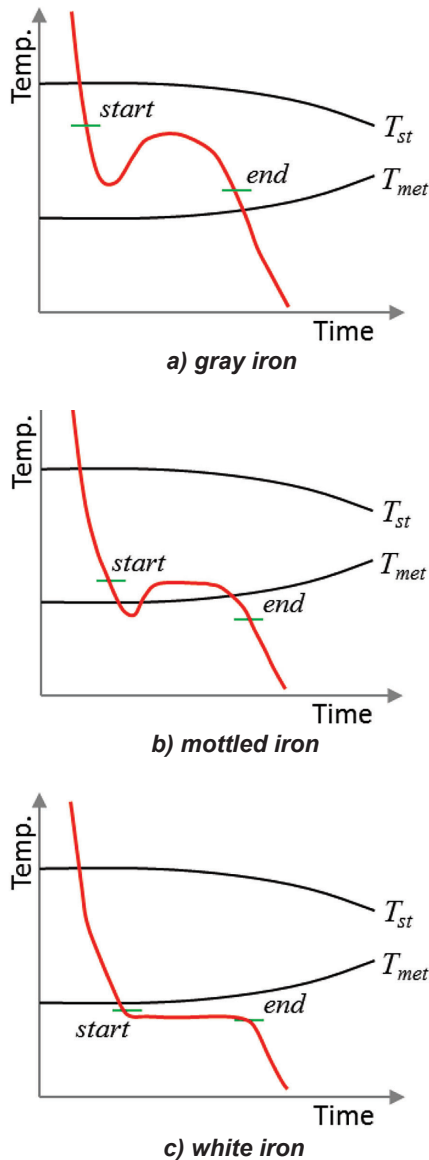


Figure 11. An interpretation of cooling curves to predict stable or metastable solidification in cast iron.

11a). If the end of solidification is under T_{met} the iron is mottled (mixed gray and white, Fig. 11b). If both the beginning and end of solidification are under T_{met} , the iron is white (Fig. 11c). Note that T_{st} and T_{met} are not straight line, because they reflect the effect of solute build-up or depletion during solidification. Carbide promoting elements are rejected in the liquid, their content increases, and T_{met} goes up. The opposite is true for graphite promoting elements.

Various inoculation additions to the iron greatly affect the eutectic temperature. As shown in Fig. 12, the addition of 0.002% Bi lowers the T_{Emin} by 9°F (5°C), and raises the T_{Emax} by 3°F (1.7°C). A combined addition of 0.002% Bi and a commercial inoculant in the sprue raised the T_{Emin} by 25°F (14°C).¹⁸

The degree of inoculation of LG iron can be estimated by using two cups: one before inoculation, and one after inoculation. The ratio $(\Delta T_{max})_{before}/(\Delta T_{max})_{after}$ steadily increases with better inoculation (higher number of eutectic grains), as shown schematically in Fig. 5.

Kanno et al.¹⁹ used three cups with one thermocouple each to predict the eutectic graphitization ability of LG iron. They defined the eutectic graphitization ability, EGA, through the equation (see Fig. 13 for definitions):

$$EGA = \frac{DT1}{DTE} = \frac{T_{Emin}(base\ iron) - T_{Emin}(Te\ cup)}{T_{Emax}(inoc.\ iron) - T_{Emin}(Te\ cup)} \quad \text{Eqn. 4}$$

Here, DTE symbolizes the difference between the stable and metastable eutectic temperatures. $DT1$ is the difference between the maximum eutectic temperature of the inoculated iron and the metastable temperature. As shown in Figure 14, there is a clear correlation between EGA , the type of graphite and the chill depth. A good correlation was also found between EGA and the tensile strength, as follows:

$$TS = (180 \cdot EGA + 170) \cdot (4.4 - CE) + 160 \quad \text{Eqn. 5}$$

Where; TS is the tensile strength.

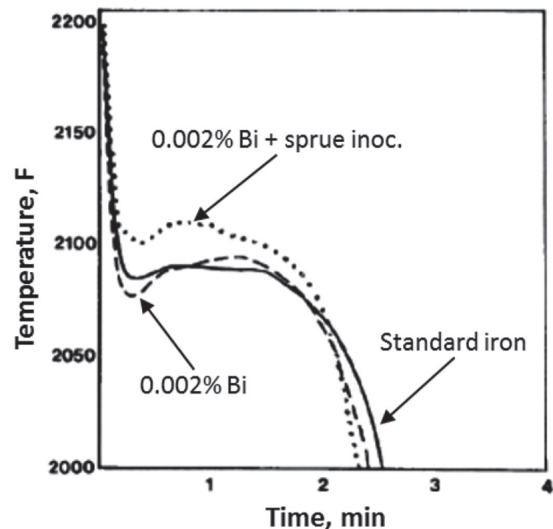


Figure 12. Effect of Bi inoculation on SG iron.¹⁸

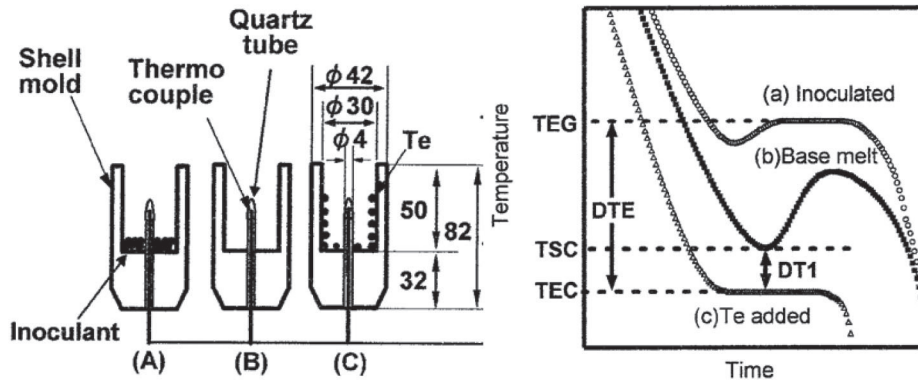


Figure 13. Three-thermocouple thermal analysis of gray iron.¹⁹

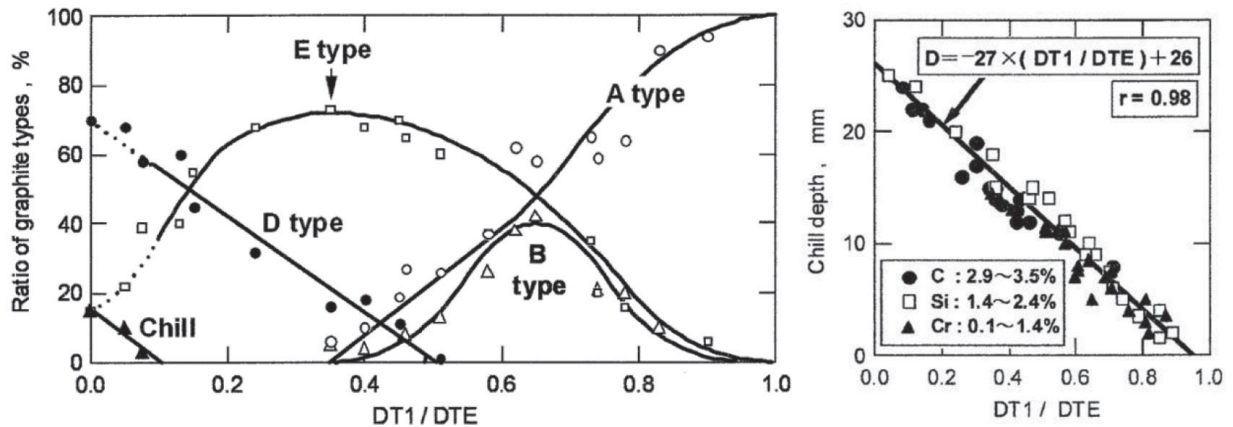


Figure 14. Correlation between the eutectic graphitization ability, type of lamellar graphite and chilling tendency in lamellar graphite iron.¹⁹

Prediction of Graphite Shape

One of the early objectives of TA as applied to cast iron was prediction of nodularity in ductile iron, with work being done both in industry (e.g., Ref. 20, 21 and in academia²²). One direction of research focused on the shape of the cooling curve (Fig. 15). Another approach was to correlate various temperature data with elements of the microstructure (Fig. 16). This last method was later extended to the prediction of compacted graphite iron structure by correlating the eutectic temperature and the recalescence to the graphite morphology, as summarized in Fig. 17.^{10,23} None of these early approaches were deemed accurate enough for process implementation on the foundry floor.

As early as 1972, a new technique became available for TA interpretation when Rabus and Polten²⁴ used computer generated cooling rates from cooling curve data (first derivative of the temperature-time curve). Derivative calculus permits the study of the rate of change, and thus of the beginning and end of transformations. Researchers used combinations of critical temperature and cooling rate to try to predict graph-

ite shape (e.g. Ref. 10, 25, 26). A second derivative of the $T-t$ curve was then calculated and studied^{27,28} (see example in Fig. 18), and then higher order derivatives, as high as the 5th derivative by Sparkman,^{29,30} were interpreted with more or less success. While the physical meaning of the first and second derivatives is clear, that of the higher order derivatives is not.

Elements of the second derivatives have been used to predict microstructure in cast iron and aluminum alloys. For example, the following relationship was derived through statistical analysis of the experimental data²⁸ for hypereutectic (CE = 4.5-4.9) thin wall LG and CG irons with Mg = 0.006-0.031%:

$$SN = -350 - 50.2 \cdot (dT/dt)_{max} + 3.31 \cdot \Delta t_{end} \quad \text{Eqn. 6}$$

with $R^2=0.87$

Where; SN sphericity nodularity defined by:

$$Sphericity (S) = \frac{4\pi \cdot Area}{(perimeter)^2}$$

$$Sphericity Nodularity (Area) = \frac{Area \text{ of acceptable particles} \cdot 100}{Area \text{ of (acceptable+unacceptable particles)}}$$

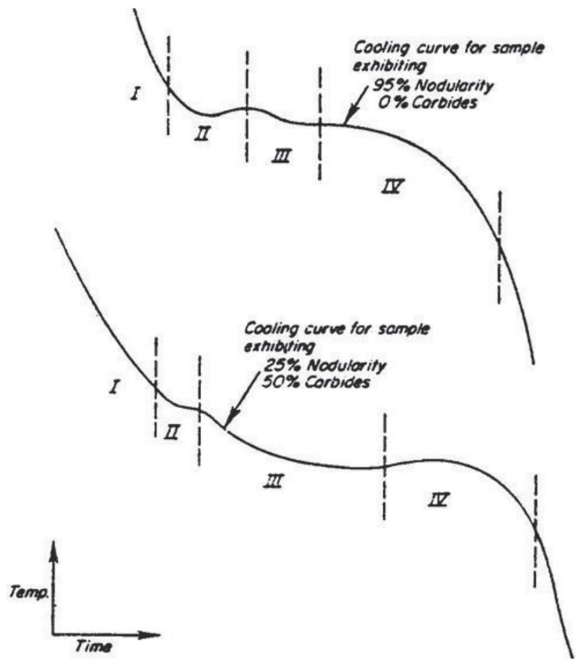


Figure 15. Correlation between the shape of the cooling curves and nodularity.²⁰

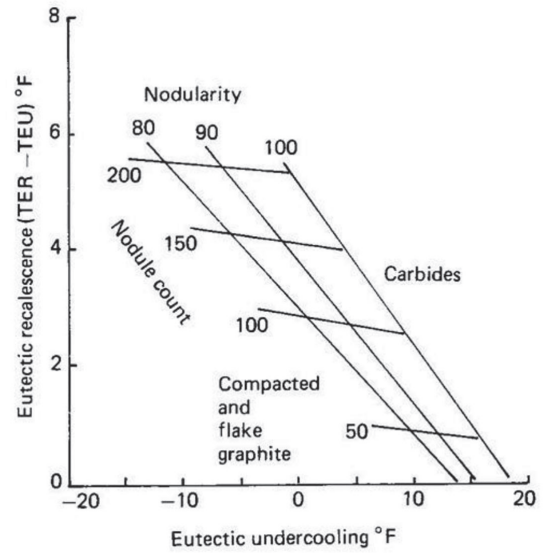
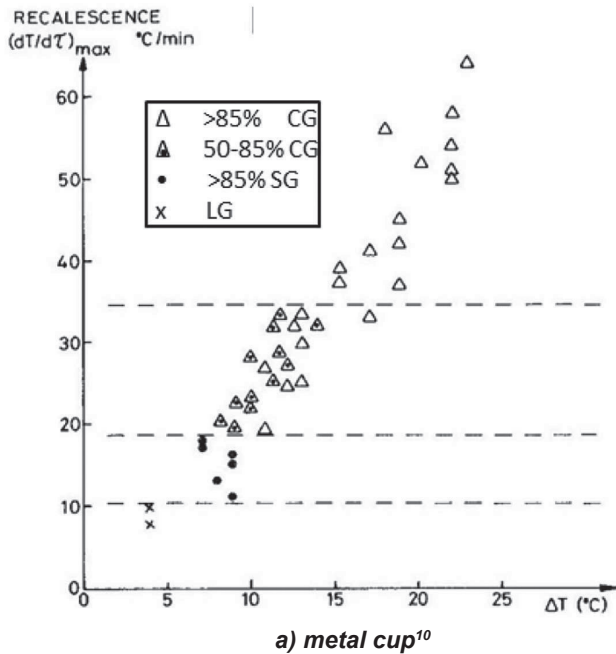
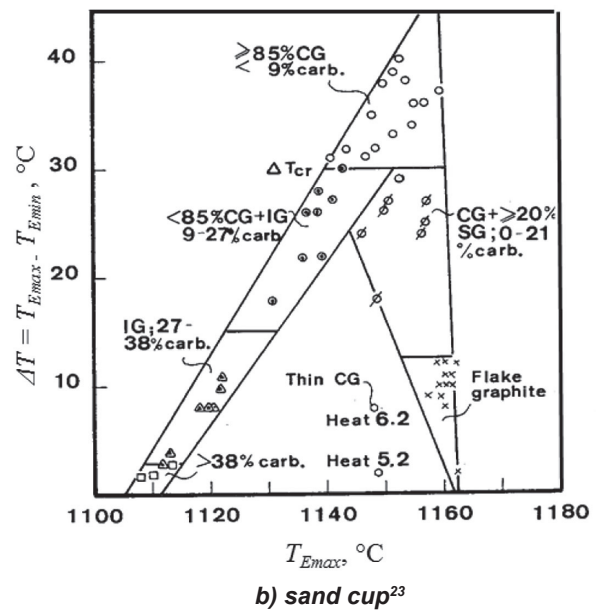


Figure 16. Correlation between temperatures on the cooling curve and microstructure of SG iron.²²



a) metal cup¹⁰



b) sand cup²³

Figure 17. Correlation between temperatures on the cooling curve and microstructure of CC iron.⁴¹

Bäckerud et al.³⁸ suggested the use of the maximum of the first derivative in the region of primary solidification of alu-

minum alloys, and the area under it, for the estimation of the efficiency of grain refinement (Fig. 19).

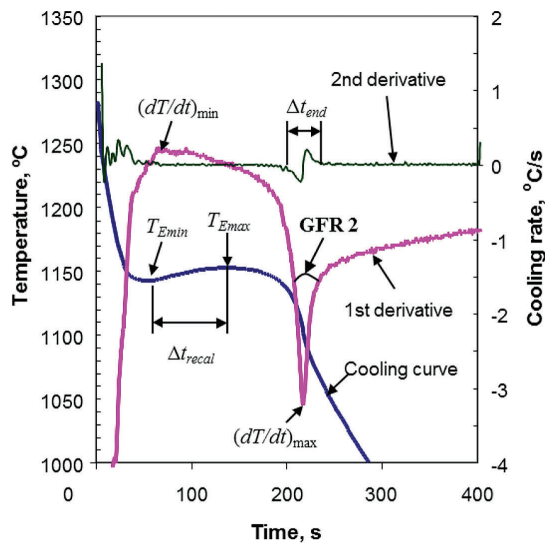


Figure 18. Cooling curve, first derivative and second derivative.²⁸

Prediction of Shrinkage Propensity

Some commercial software programs have used the angle of the cooling rate curve at the end of solidification, GFR 2 in Fig. 18, as an indicator of the microshrinkage propensity in cast iron, a large angle suggesting a high shrinkage tendency.³¹ This is because the differences in the skin-type solidification of LG iron and the mushy-type solidification of SG iron. Very little latent heat is released at the end of solidification of LG iron which determines a sharp increase in the cooling rate. More latent heat is released at the end of solidification of SG iron, resulting in slower increase in the cooling rate. As shown in the example in Fig. 20, the lamellar graphite iron has a higher cooling rate and a narrower angle at the end of solidification when compared with the spheroidal graphite iron.

The use of the first derivative of the T-t curve allows estimation of the time at which various solidification events are occurring. According to Larrañaga et al.,³² the ratio

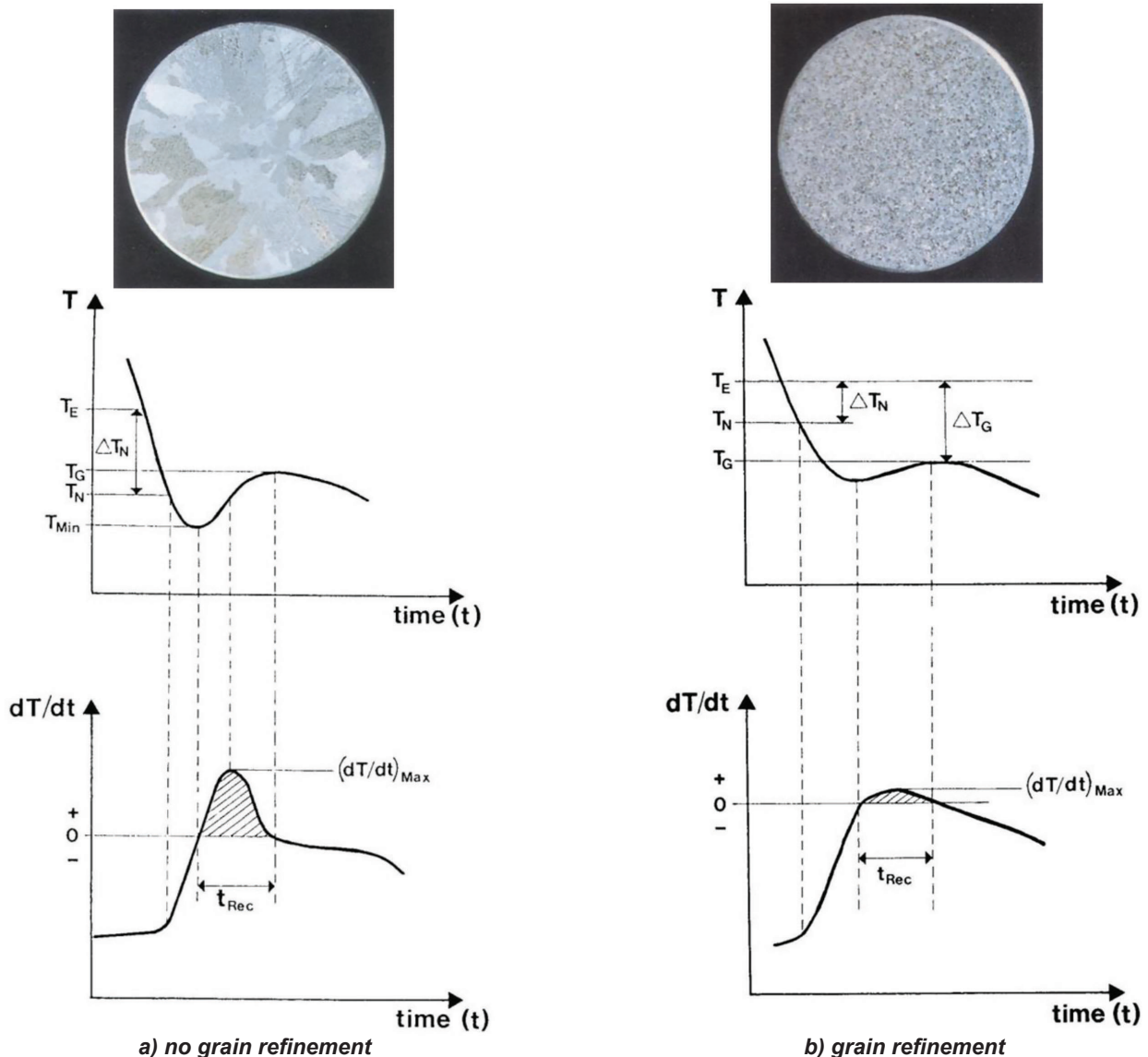


Figure 19. Interpretation of the cooling curve and its first derivative to estimate grain refinement in aluminum alloys.³⁸

$k = t_{EXP} / (t_{Exp} + t_{Final, contr.})$ can use as a predictor for shrinkage porosity in cast iron (see Fig. 21 for definitions). A low k is an indicator of high porosity. The same authors have also proposed an empirical equation for the calculation of nodule count based on TA data.

Prediction of Degree O Oxidation of the Melt

Increased oxygen in the range of 11-101 ppm in an iron melt of composition 3.39-3.46%C and 1.38-1.58%Si has been reported to raise the liquidus temperature by as much as 10°C (18°F).³³ Inoculation lowered the T_{LA} . Similar effects were noticed for steel where dissolved oxygen raised T_{LA} and de-oxidation with Al depressed T_{LA} .³⁴

Heine and Henschel^{14,35} conducted experiments on a large number of melts to find the effect of oxygen on the TLA of iron melts. For melts deoxidized under argon they derived Eqn. 2. For melts under oxidizing atmosphere the equation was:

$$T_{LA} = 1594.4 - 102.2(\%C + 0.25\%Si + 0.5\%P) \quad \text{Eqn. 7}$$

For melts superheated at 1510°C (2750°F) the equation was:

$$T_{LA} = 1550 - 92.06(\%C + 0.25\%Si + 0.5\%P) \quad \text{Eqn. 8}$$

These three equations were plotted in Fig. 22. It was confirmed that the oxygen increases T_{LA} . This effect may be understood on the basis of thermodynamics. Oxygen lowers carbon activity, which is equivalent to a decrease in carbon in terms of solidification behaviour. This implies an increase in the temperature. Superheating decreases the liquidus, most probably because it decreases the nucleation potential of the melt.

Prediction of Mechanical Properties

Attempts have also been made to predict mechanical properties using TA data by Kano et al.¹⁹ (Eqn. 5) as already discussed in this paper. Earlier, Glover et al.³⁶ performed regression analysis on a large number of samples and obtained the following correlation between tensile strength (TS in psi) and the liquidus arrest (in °C):

$$TS = -388,447 + 357 \cdot T_{LA} \quad (R^2 = 55) \quad \text{Eqn. 9}$$

The poor correlation coefficient is not surprising, as essential microstructure features such as graphite shape, amount of dendrites, dendrite arm spacing, and eutectic grain size have a rather complex or little influence on the liquidus temperature. To improve the correlation Glover et al. introduced into the analysis the *dendrite interaction area* which represents a qualitative estimate of the area fraction of dendrites. The new equation had a higher correlation coefficient, but was still insufficient for reliable prediction for the tensile strength:

$$TS = -248,504 + 234 \cdot T_{LA} + 93(\% \text{ Dendrite Interaction}) \quad (R^2 = 72) \quad \text{Eqn. 10}$$

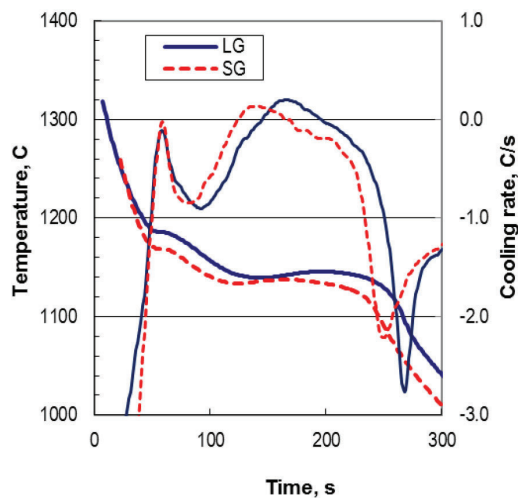


Figure 20. Comparison of the end of solidification for ductile (SG) and gray (LG) irons.

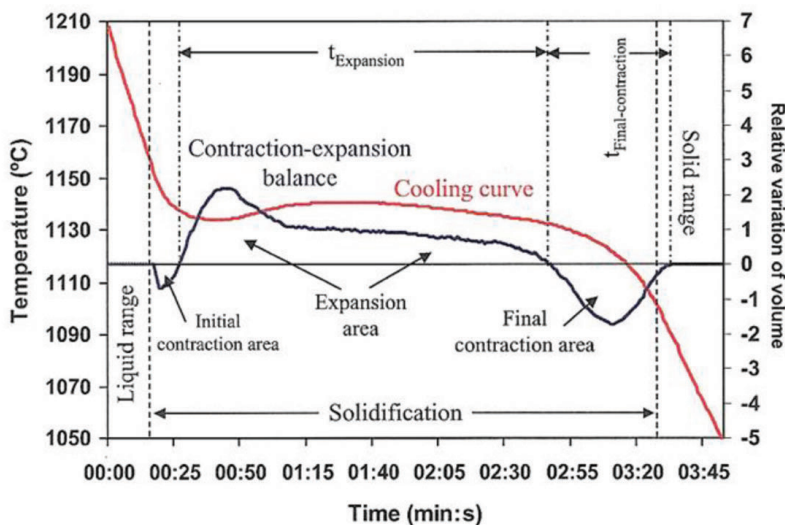


Figure 21. Suggested correlation between times and areas from the cooling and cooling rates curves to microporosity propensity in cast iron.³²

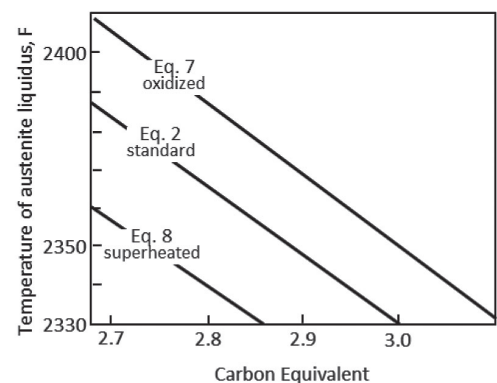


Figure 22. Effect of oxygen and superheating on the liquidus temperature (Heine).

Differential Thermal Analysis (DTA)

DTA with a Reference Sample

Classic DTA is performed with a reference body (Fig. 23a). The sample and the reference body are cooled at a controlled, constant speed via the furnace. An example of the interpretation of the cooling curves is given in Fig. 23b for high speed steel. At the beginning of cooling the temperature of the sample (T_{sam}) and of the reference (T_{ref}) follow parallel paths. When an exothermic reaction, such as a phase change occurs, the temperature will increase and a peak will form on the sample temperature graph. In this case the sudden increase in temperature was produced by the latent heat released because of the solidification of the δ -phase. Similar effects are seen for the peritectic reaction and the eutectic solidification. The areas above the straight line are proportional with the latent heat released during the phase transformation. An endothermic peak may occur during cooling when a crystalline phase change occurs.

To calculate the latent heat produced during the transformation, we start with the heat flow rate balance of the test - casting/crucible system:

$$\frac{dQ_f}{dt} - v\rho c_p(dT/dt)_{sam} = hA(T_{sam} - T_o) + \varepsilon\sigma(T_{sam}^4 - T_o^4) \quad \text{Eqn. 11}$$

Where;

- Q_f is the solidification latent heat;
- t is the time;
- v is the sample volume;
- ρ is the metal density;
- c_p is the specific heat of the metal;
- T is the average temperature in the sample;
- h is the effective heat transfer coefficient;
- A is the surface area of the sample;
- T_o is the furnace temperature;
- ε is the emissivity of the surface sample;
- σ is the Stefan-Boltzmann constant.

It can be shown that, after some manipulations, the time evolution of the latent heat can be calculated as:

$$\frac{dQ_f}{dt} = v\rho c_p \left[(dT/dt)_{sam} - (dT/dt)_{ref} \right] + hA(T_{sam} - T_o) + \varepsilon\sigma(T_{sam}^4 - T_o^4) \quad \text{Eqn. 12}$$

The total latent heat evolved during solidification, Q_f , can be obtained from the time integration of this equation. The reaction rate (rate of fraction of solid evolution) can then be calculated through the numerical integration of:

$$f_s^i = f_s^{i-1} + Q_f^i / Q_f \quad \text{Eqn. 13}$$

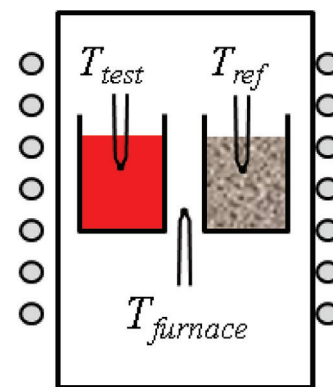
Where; f_s^i is the fraction solid generated from time zero to time t_i , and Q_f^i is the total heat generated till time i .

This method is widely applied in research laboratories, but it is not directly used in metalcasting processing because it

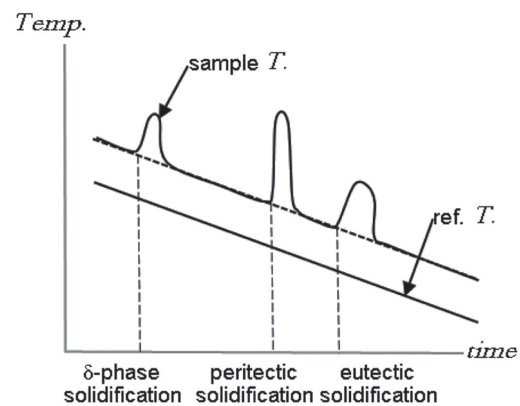
cannot provide timely data useful in operation. For a more in depth discussion on classic DTA the reader is referred to Ref. 37.

Bäckerud et al.³⁸ experimented with a modified DTA in which the reference sample was not a neutral body, but a second thermocouple placed in the same cup, close to the wall. Two cooling curves were thus recorded for the same alloy (Fig. 24a). The temperature difference between the wall and center thermocouples that describes the temperature gradient across the sample can be used to determine the occurrence of solidification events such as nucleation at wall, dendrite coherency, and formation of various phases such as Mg_2Si (Fig. 24b).

A successful industrial process based on the two-thermocouple DTA method is the SinterCast process for production of CG iron.³⁹ It uses a stamped and drawn steel sheet cup that has a spheroidal containment area (Fig. 6b). The cup is immersed in the molten iron. Two different cooling curves are obtained from two thermocouples protected by the same sheath. One of the thermocouples is located in the thermal center of the cup while the second is located close to the bottom of sample. The walls of the cup are coated with a reactive coating that consumes active magnesium in order



a) equipment for DTA



b) interpretation of DTA

Figure 23. Schematic representations of the principles of DTA.

to simulate the fading of magnesium in the ladle. This allows for the simultaneous measurement of the solidification behavior at the start of casting (through the center thermocouple) and also after a predetermined loss of magnesium (through the bottom thermocouple). Computer-aided cooling curve analysis allows the prediction of the solidification microstructure of the iron and, more importantly, the corrections necessary to achieve the desired CG microstructure.

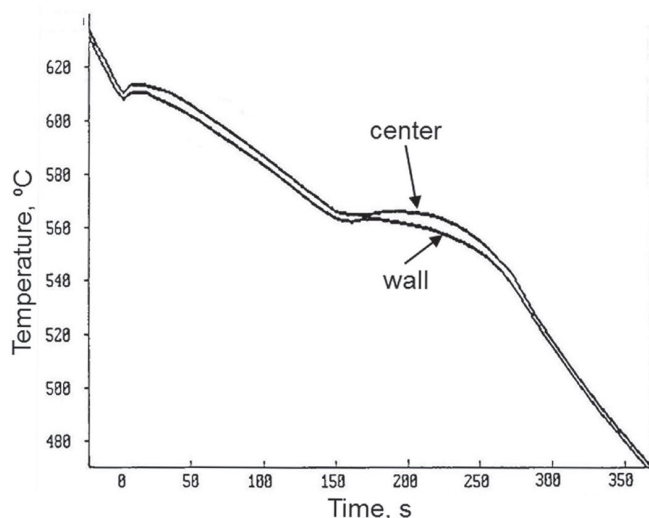
DTA Without a Reference Sample

Integral calculus applied to the temperature-time data allows evaluation of areas that are directly related to the energy evolution. DTA lends itself to straight forward integral calculus analysis. DTA can also be conducted without a reference sample. In this case, a test cup with one thermocouple is used. The problem is then to calculate the cooling of the virtual reference sample. There are in principle two major approaches: i) Newtonian analysis and ii) Fourier analysis. Newtonian analysis requires only one thermocouple and is the most widely used. The mathematics is straight forward (see References 40-47). Fourier analysis is a more accurate treatment of the heat transfer problem, but it requires two thermocouples and the mathematics is more cumbersome (see References 48-50).

Newtonian Analysis

In the Newtonian analysis it is assumed that the thermal gradient across the sample is zero and that heat transfer between the casting and the mold occurs by convection. The mathematical background^{40,41} is similar with that for the DTA with a reference sample, with some simplifications. Assuming that the heat loss by radiation is negligible during solidification, Eqn. 11 becomes:

$$\frac{dQ_f}{dt} - v\rho c_p \left(\frac{dT}{dt} \right)_{cc} = h_{cc} A (T_{cc} - T_o) \quad \text{Eqn. 14}$$



a) cooling curves

Where the subscript *cc* designates the cooling curve and T_o is the ambient temperature. The thermo-physical quantities are assumed constant. The equation can be rearranged to describe the cooling rate:

$$\left(\frac{dT}{dt} \right)_{cc} = \frac{1}{v\rho c_p} \left[\frac{dQ_f}{dt} - h_{cc} A (T_{cc} - T_o) \right] \quad \text{Eqn. 15}$$

If no phase transformation occurs during cooling $Q_f = 0$ and the equation becomes:

$$\left(\frac{dT}{dt} \right)_{zc} = - \frac{h_{zc} A (T_{cc} - T_o)}{v\rho c_p} \quad \text{Eqn. 16}$$

Here the subscript *zc* denotes the zero-curve, which is the time evolution of the alloy cooling rate assuming no phase transformation, *i.e.*, the cooling rate of the virtual reference sample. This is the cooling rate of the virtual reference (neutral) body. Assuming that $h_{cc} = h_{zc}$ the time evolution of the latent heat can be calculated as:

$$\frac{dQ_f}{dt} = v\rho c_p \left[\left(\frac{dT}{dt} \right)_{cc} - \left(\frac{dT}{dt} \right)_{zc} \right] \quad \text{Eqn. 17}$$

and the total heat evolution during solidification is:

$$Q_f = v\rho c_p \int_{t_{start}}^{t_{end}} \left[\left(\frac{dT}{dt} \right)_{cc} - \left(\frac{dT}{dt} \right)_{zc} \right] dt \quad \text{Eqn. 18}$$

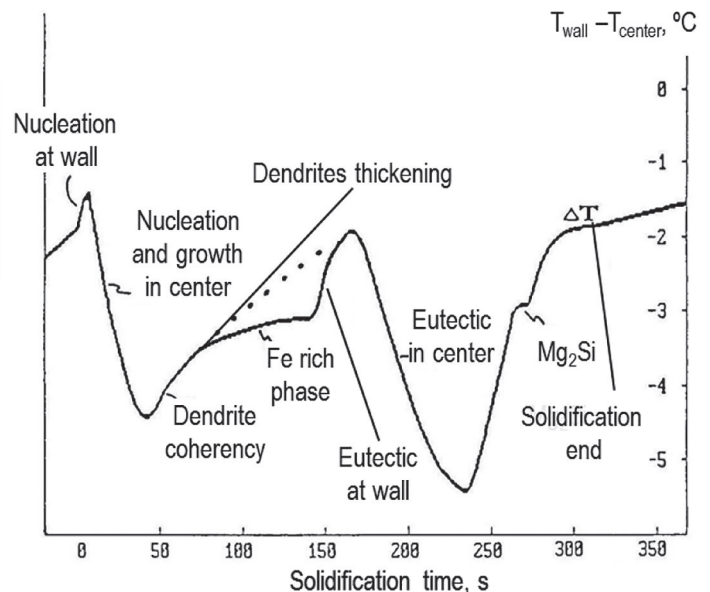
The latent heat can be calculated by numerical integration of this equation:

$$Q_f = v\rho c_p \left[\text{area under } \left(\frac{dT}{dt} \right)_{cc} - \text{area under } \left(\frac{dT}{dt} \right)_{zc} \right] \quad \text{Eqn. 19}$$

The fraction solid at time *i* is then calculated with Eqn. 13, or as:

$$f_s^t = \frac{Q_f^t}{Q_f} = \frac{v\rho c_p \int_{t_{start}}^t \left[\left(\frac{dT}{dt} \right)_{cc} - \left(\frac{dT}{dt} \right)_{zc} \right] dt}{Q_f} \quad \text{Eqn. 20}$$

The problem can now be solved on the Excel spreadsheet.



b) temperature difference between wall and center

Figure 24. DTA with two thermocouples in the same sample.³⁸

In principle the method consists in generating the first derivative of the cooling curve with respect to time (the cooling rate), generating a zero-curve, and then subtracting the area under the zero-curve from the area under the cooling rate. There is no unique accepted method to obtain the zero-curve.

The example in Fig. 25 is for a hypoeutectic cast iron. Once the zero-curve is known, the time evolution of the phase transformation is obtained by dividing the area corresponding to the phase formation (for example area corresponding to the solidification of primary austenite) to the total area, the evolution in time of the amount of this phase is obtained. In the example in Fig. 25, if the beginning of eutectic solidification is known, the amount of primary austenite and the amount of eutectic can be calculated. Then, the evolution of fraction solid over the solidification time can be plotted.

There are two problems in the Newtonian analysis: i) establishing the beginning and the end of the austenite and eutectic solidification and ii) calculating the zero-curve. Many papers suggest the use of the first derivative to establish the beginning and end of transformation. However, we have demonstrated that this is inaccurate. The beginning and end of a phase transformation is best obtained from the second derivative of the cooling curve.⁵¹ This is because a maximum of the second derivative indicates a sudden decrease in the cooling rate corresponding to phase solidification, while a minimum on the second derivative indicates a sudden increase in the cooling rate corresponding to the end of any solidification (no latent heat production). Figure 26 shows a cooling curve in the region of the eutectic transformation of an LG iron. The maximum of the 2nd derivative corre-

sponds to the beginning of the eutectic solidification, while the minimum of the 2nd derivative corresponds to the end of the eutectic solidification.

To generate the zero-curve (ZC) the heat transfer coefficient for the cooling without transformation is needed. A possible approach has been described by Ekpoom and Heine.⁴⁰ They calculated a heat transfer coefficient for the liquid stage, h_L , and for the solid stage, h_S . In the mushy zone, linear interpolation between h_L and h_S is used. The method is cumbersome.

Alternatively, the heat transfer coefficient (h) can be generated from the cooling curve or its first derivative. Barlow and Stefanescu⁴⁹ proposed the use of a fitted exponential on the cooling rate before and after solidification, which meant using one heat transfer coefficient over the entire measuring interval. Another procedure was to use three heat transfer coefficients by fitting exponentials for points on the cooling rate before the beginning of solidification, after the end of solidification, and another one between the points corresponding to the beginning and end of solidification.

In principle, three approaches can be used to compute the zero line (Fig. 27):

1. ZC1h: logarithmic trend line for points chosen at the beginning and the end of the cooling rate (CR) curve; this method uses only one heat transfer coefficient for the entire cooling curve.
2. ZC2h: logarithmic trend line for one point on the CR corresponding to the beginning of the austenite solidification (the maximum of the 2nd derivative) and points at the end of the CR curve; while only one h is needed for the calculation of the transfor-

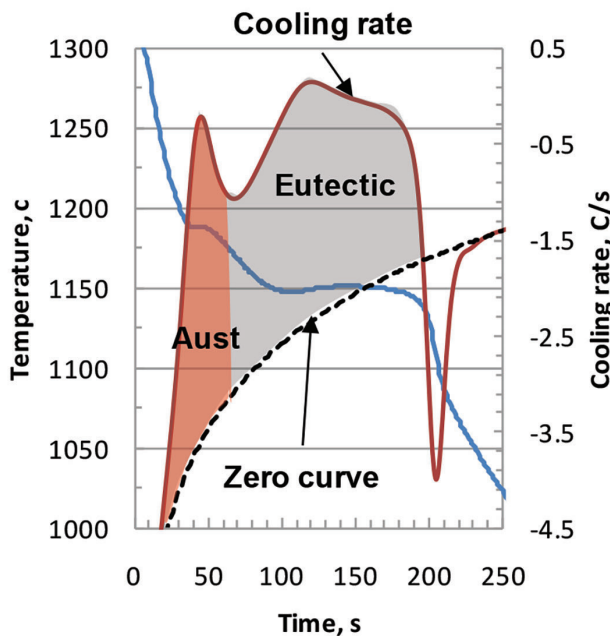


Figure 25. Calculation of the amount of phases from the areas under the cooling rate and the zero curves.

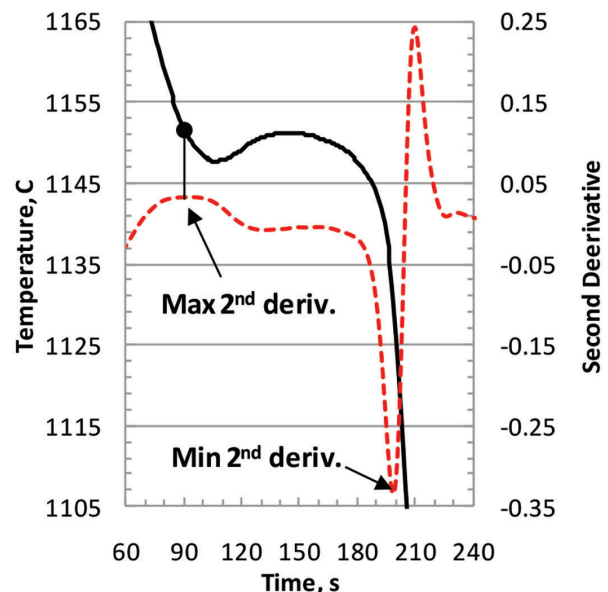


Figure 26. The use of the 2nd derivative to establish the beginning and the end of eutectic solidification.

mation region of the ZC, two are needed for the whole ZC.

3. ZC3h: logarithmic trend line for points on the CR corresponding to the beginning and end of the austenite solidification.

Once the ZC is generated, a normalized cooling rate (NCR) can be plotted. It is the difference between the area under the cooling rate curve and that under the ZC (see Fig. 28). The normalized cooling rate covers only the solidification part of the cooling curve. The area under the normalized CC is proportional to the latent heat of solidification. The evolution of the fraction austenite and total fraction solid can then be calculated and plotted.

Calculated fraction solid obtained from a single-thermocouple Newtonian TA could have significant departure from data obtained through computational modeling of the specimen when the specimen cooled at high Biot number. To increase the precision of TA for cast steel, Lekakh and Richards⁴⁶ used a pre-heated thermally insulated ceramic mold. Fraction solid and dendrite coherency point were evaluated.

Fourier Analysis

Fourier analysis assumes that heat transfer takes place by conduction only. The following analysis⁴⁹ closely follows the method suggested by Fras et al.⁴⁸ The Fourier equation with a heat source term is:

$$\frac{\partial T}{\partial t} = \alpha \nabla^2 T + \frac{1}{c_p} \frac{\partial Q_f}{\partial t} \quad \text{or} \quad \frac{\partial Q_f}{\partial t} = c_p \left(\frac{\partial T}{\partial t} - Z_F \right) \quad \text{Eqn. 21}$$

with the zero curve given by $Z_F = \alpha \nabla^2 T$. To calculate this curve we must know the temperature field, which for a cylindrical

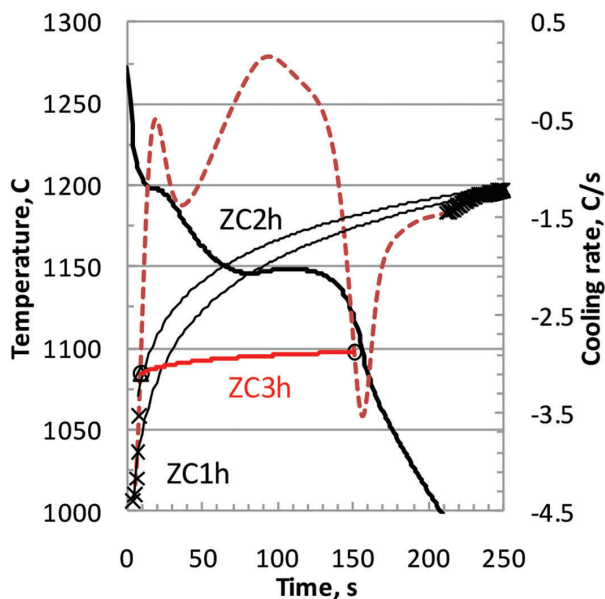


Figure 27. Three methods of generation of the zero curve.⁵¹

mold can be calculated as $\nabla^2 T = 4(T_2 - T_1)/(r_2^2 - r_1^2)$, where T_2 and T_1 are the temperatures at radii r_2 and r_1 , respectively. This introduces the need for two thermocouples. The thermo-physical quantities are time and temperature dependent. The latent heat and fraction solid evolution are calculated as described for the Newtonian analysis. Typical results are shown in Fig. 29 for an aluminum alloy. The time close to the end of solidification, when the cooling curve and the Fourier zero curve start coinciding, is considered the end of solidification. Note that this occurs earlier than the minimum at the end of the cooling curve.

Mathematically, the Fourier analysis is more accurate than the Newtonian analysis, but its experimental application is more onerous because the two thermocouples must be positioned accurately in the measuring cup, an almost impossible task for sand cups. A more detailed analysis of the Fourier method through inverse heat conduction analysis was offered by Diószegi and Hattel.⁵⁰

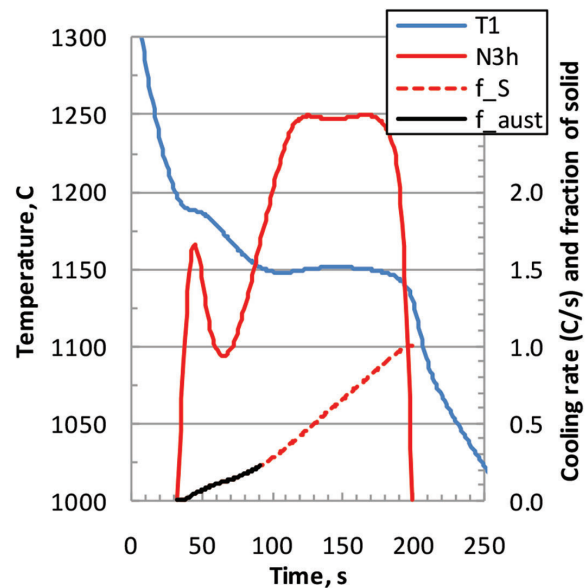


Figure 28. Normalized cooling rate (N3h) and the evolution of the solid and primary austenite fractions.⁵¹

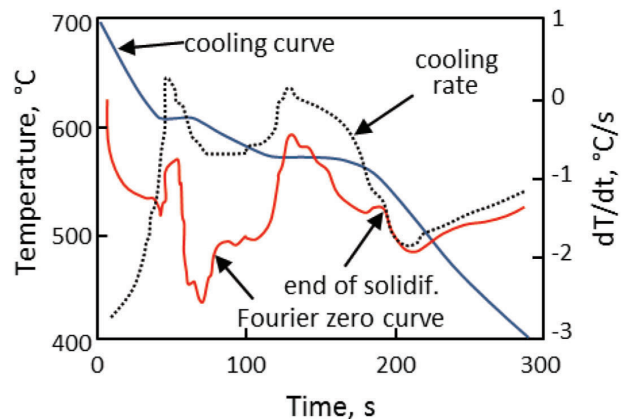


Figure 29. Cooling curve, cooling rate and Fourier zero curve for an aluminum alloy.⁴⁹

Data Smoothing Techniques

An important issue that directly impacts the accuracy and interpretation of the DTA is the smoothing of the temperature-time data. While there are many smoothing techniques, some of them proprietary, the most common ones are data averaging, Gaussian smoothing, and polynomial interpolation.

The simplest technique to implement on the Excel spreadsheet is data averaging (also known as mean filter) where in one-dimension the value of a property T over an interval $(i - j)$ is calculated as $T_{i-j} = \sum_j T / (i - j)$. An example of smoothing through averaging using an interval $i - j = 9$ is provided in Fig. 30. While no significant differences are noticeable on the cooling curve, the effect of smoothing on the cooling rate is marked. Note that some displacement of the maxima and minima occurs.

Another technique is the Gaussian smoothing. It is similar to the mean filter but uses the Gaussian distribution $G(x) = (\sqrt{2\pi}\sigma)^{-1} e^{-x^2/2\sigma^2}$, where σ is the standard deviation of the distribution, to perform the smoothing. The two techniques are compared in Fig. 31. A Gaussian smoothing add-on for the Excel spreadsheet was used for the calculation.

The polynomial interpolation is a simple mathematical procedure that involves fitting of a data set through a polynomial equation of a selected order. An example of fitting experimental data with a 10th order polynomial is presented in Fig. 32. A higher order polynomial will provide a better match of the experimental cooling curve. The advantage of this method is that the data is completely smooth, facilitating the detection of the critical points on the cooling curve.

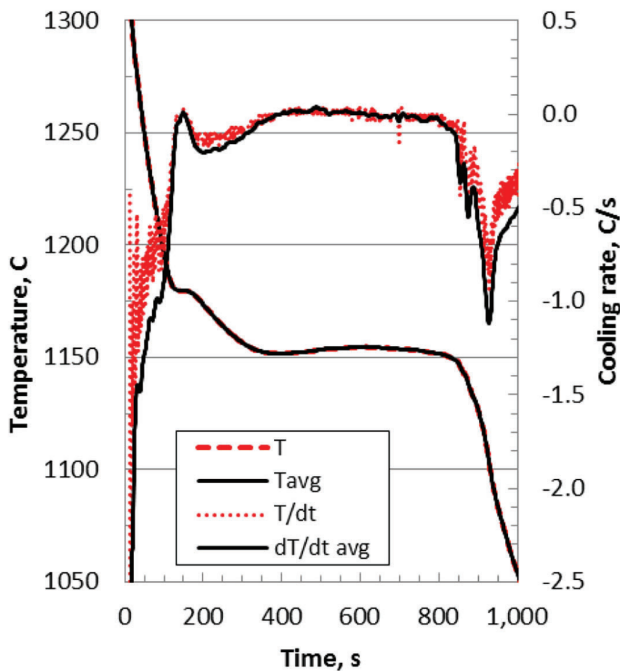


Figure 30. Comparison between the raw data (dotted lines) and data smoothed by averaging over 9 points (full lines).

Conclusions

Thermal analysis of casting alloys in its direct form or as differential thermal analysis can provide information about the composition of the alloy, the latent heat of solidification, the evolution of the fraction solid, the amounts and

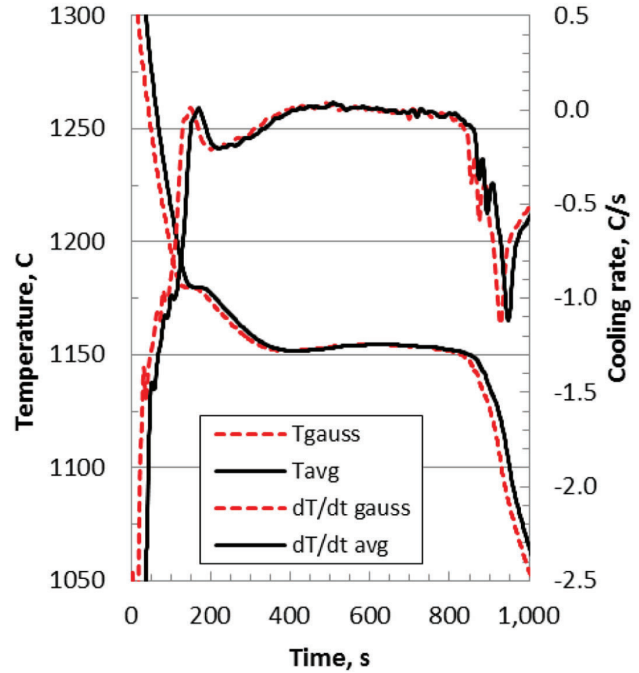


Figure 31. Comparison between Gaussian smoothing (dotted lines) and averaging smoothing (full lines). The data for averaging have been displaced to the right by 20s on purpose, to facilitate observation of differences.

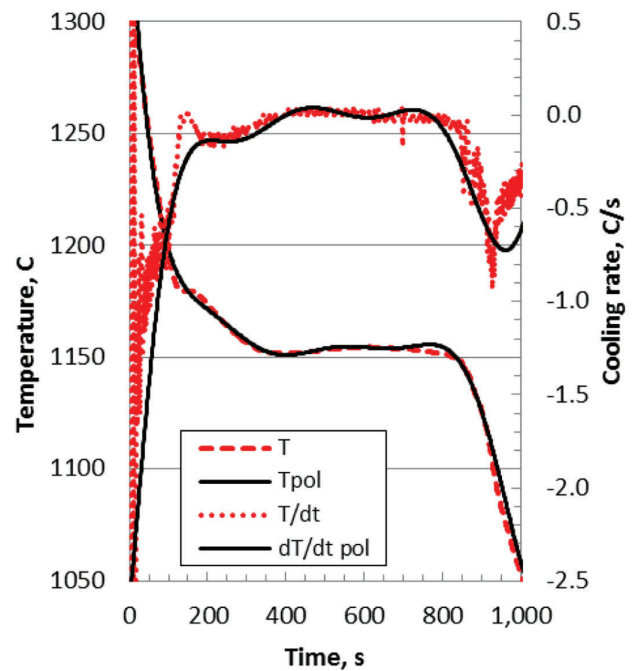


Figure 32. Comparison between the raw data (dotted lines) and data smoothed by 10th order polynomial interpolation (full lines).

types of phases that solidify, and even dendrite coherency. There are also many other uses for TA, such as, determining dendrite arm spacing in aluminum alloys (e.g., References 52,53) and steel,⁴⁶ degree of modification and grain refining in aluminum alloys (e.g., References 54-57 in addition to work already cited), graphite morphology and the degree of nodularity in cast irons (e.g., References 58,59 in addition to work already cited), and even determining the most effective heat treatment cycle for the production of austempered ductile iron.⁶⁰ The use of TA for process control in metalcasting is very extensive and dynamic ongoing, with improved in equipment and data analysis.

The metalcaster should be aware that the vast majority of the information provided by the commercial software for TA and DTA is based on empirical equations obtained through statistical analysis, as shown through examples in this paper. Therefore, the input of the plant metallurgist is a necessary prerequisite for confidence building in the tools used for TA.

REFERENCES

- H. Le Chatelier, *Z. Phys. Chem.* 1 (1887) 396.
- W.C. Roberts-Austen, *Metallographist*, 2 (1899) 186.
- N.S. Kurnakov, *Z. Anorg. Chemie*, 42 (1904) 184.
- E. Saladin, *Iron and Steel Metallurgy Metallography*, 7 (1904) 237.
- E. Piwowarski, *Hochwertiges Gusseisen*, Springer Verlag, Berlin (1961).
- E. Piwowarski, *Giesserei* 25 (1938) 523.
- C.R. Loper, R.W. Heine and A. Shah, *AFS Trans.* 75 (1967) 541.
- R.L. Naro and J.F. Wallace, *AFS Trans.* 78 (1970) 229-238.
- A. De Sy, J. Vidts, *Traité de metallurgie structurale theorique et appliquée*, Ed. Dunod, Paris (1962) 464p.
- L. Bäckerud, K. Nilsson and H. Steen, in *The Metallurgy of Cast Iron*, B. Lux, I. Minkoff and F. Mollard, Eds., Georgi Publishing, Switzerland (1975) 625.
- D.M. Stefanescu, in *The Physical Metallurgy of Cast Iron*, H. Fredriksson and M. Hillert eds., Elsevier (1985) 151.
- J.G. Humphreys, *BCIRA J.* 9 (1961) 609-621.
- D.M. Stefanescu and S. Katz, "Thermodynamic Properties of Iron-Base Alloys," *ASM Handbook vol. 15 – Casting* (2008) 41-55.
- R.W. Heine, *AFS Cast Metals Res. J.* (June 1971) 49-54.
- R.W. Heine, *AFS Trans.* 82 (1974) 462-470.
- W. Donald and A. Moore, BCIRA Report no. 1128 (1973).
- W. Van der Perre: "Thermal analysis, principles and applications," Heraeus Electro-Nite website <http://heraeus-electro-nite.com> (last accessed 10-30-14).
- G.R. Strong, *AFS Trans.* 91 (1983) 151-156.
- T. Kanno, I. Kang, Y. Fukuda, M. Morinaka and H. Nakae, *AFS Trans.* (2006) paper 06-083.
- E.F. Ryntz, J.F. Janowak, A.W. Hochstein and C.A. Wargel, *AFS Trans.* 79 (1971) 161-164.
- R. Monroe and C.E. Bates, *AFS Trans.* 90 (1982) 307-311.
- M.D. Chaudhari, R.W. Heine and C.R. Loper, *AFS Trans.* 79 (1971) 399.
- D.M. Stefanescu, C.R. Loper, R.C. Voigt and I.G. Chen, *AFS Trans.* 90 (1982) 333.
- D. Rabus and S. Polten, *Giesserei Rundschau*, no. 9 (1972) 1-8.
- P. Strizik, *Giesserei* 61 (1974) 615-618.
- D.M. Stefanescu, L. Dinescu, S. Craciun and M. Popescu, in *Proc. 46th Int. Foundry Cong.*, Madrid, Spain, CIATF, (October 1979).
- I.G. Chen, D.M. Stefanescu, *AFS Transactions*, 92 (1984) 947-964.
- S. Charoenvilaisiri and D. M. Stefanescu, *Proceedings of the 7th Asian Foundry Congress*, Taipei, Taiwan (2001) 91.
- D.A. Sparkman, "Thermal Analysis Metrics by Derivatives," <http://www.meltlab.com/hottopics/feb2010htopic.pdf> (last accessed 10-30-14).
- D.A. Sparkman, *Trans. AFS* 119 (2011).
- P.E. Persson, A. Udroui, P. Vomacka, Wang Xiaojing and T. Sjögren, *Proceedings of the 69th World Foundry Congress* (2010).
- P. Larrañaga, J.M. Gutierrez, A. Loizaga, J. Sertucha, and R. Suárez, *Trans. AFS* 116 (2008) paper 08-008.
- N. Kayama, K. Murai, H. Nakae, *Report Casting Res. Lab.*, Waseda Univ., Tokyo no.21 (1970).
- G. Mahn, B.C. Mahanty, *Stahl und Eisen*, 89(23) (1969).
- C. Henschel, R.W. Heine, *AFS Cast Metals Res. J.* (Sept. 1971).
- D. Glover, C.E. Bates and R. Monroe, *Trans. AFS*, 90 (1982) 745-757.
- H. Fredriksson and Ulla Åkerlind, *Solidification and Crystallization Processing in Metals and Alloys*, Wiley (2012).
- L. Bäckerud, G.C. Chai and J. Tamminen, *Solidification Characteristics of Aluminum Alloys*, AFS/Skanaluminium, Stockholm (1990) 256p.
- S. Dawson, P. Popelar, in 2013 Keith Millis Symposium on Ductile Iron (2013) 59.
- L. Ekpoom and R. W. Heine, *Trans. AFS*, 89 (1981) 27.
- I.G. Chen and D. M. Stefanescu, *Trans. AFS* 92 (1984) 947.
- S. L. Bäckerud and G. K. Sigworth, *Trans. AFS* 97 (1989) 459.
- K.G. Upadhya, D. M. Stefanescu, K. Lieu and D.P. Yeger, *Trans. AFS* 97 (1989) 61.
- W.T. Kierkus and J. H. Sokolowski, *Trans. AFS* 107 (1999) 161.
- R. Mackay, J. H. Sokolowski, R. Hasenbusch, and W.J. Evans, *Trans. AFS*, paper 03-96 (2003).

46. S. N. Lekakh and V. L. Richards, *Trans. AFS* 119 (2011) paper 11-042.
47. A. Dioszegi and I. Svensson *Mat. Sc. Eng. A* 413-414 (2005) 474.
48. E. Frás, W. Kapturkiewicz, A. Burbielko and H.F. Lopez, *Trans. AFS* 101 (1993) 505.
49. J.O. Barlow and D.M. Stefanescu, *Trans. AFS* 105 (1997) 349.
50. A. Dioszegi and J. Hattel, *Int. J. Cast Metals Research* 17 (2004) 311.
51. G. Alonso, P. Larrañaga, J. Sertucha, R. Suárez, D.M. Stefanescu, *Trans. AFS* 120 (2012) 329-35.
52. L. Ananthanarayanan, F.H. Samuel and J.E. Gruzleski, *AFS Trans.* 100 (1992) 383-391.
53. S. Gowri, *AFS Trans.* 102 (1994) 503-508.
54. D. Apelian, G.K. Sigworth and K.R. Whaler, *AFS Trans.* 92 (1984) 297-307.
55. J. Charbonnier, *AFS Trans.* 92 (1984) 907-922.
56. D. Apelian and J.J.A. Cheng, *AFS Trans.* 94 (1986) 797-808.
57. N. Tenekedjiev and J.E. Gruzleski, *AFS Trans.* 99 (1991) 1-6.
58. D. Sparkman, *AFS Trans.* 102 (1994) 229-233.
59. P. Zhu and R.W. Smith, *AFS Trans.* 103 (1995) 601-609.
60. C.H. Chang and T.S. Shih, *AFS Trans.* 102 (1994) 357-365.